
CASS: Cross Architectural Self-Supervision for Medical Image Analysis

Pranav Singh

Department of Computer Science
Tandon School of Engineering
New York University New York, NY 11202
ps4364@nyu.edu

Elena Sizikova

Center for Data Science
New York University New York, NY 10011
es5223@nyu.edu

Jacopo Cirrone

Center for Data Science
New York University
and Colton Center for Autoimmunity
NYU Grossman School of Medicine
New York, NY 10011
cirrone@courant.nyu.edu

Abstract

Recent advances in deep learning and computer vision have reduced many barriers to automated medical image analysis, allowing algorithms to process label-free images and improve performance. Specifically, Transformers provide a global perspective of the image, that Convolutional Neural Networks (CNNs) inherently lack. Here we present **Cross Architectural - Self Supervision**, a novel self-supervised learning approach that leverages Transformer and CNN simultaneously. Compared to the existing state of the art self-supervised learning approaches, we empirically showed that CASS trained CNNs, and Transformers across three diverse datasets gained an average of 8.5% with 100% labelled data, 7.3% with 10% labelled data, and 11.5% with 1% labelled data. Notably, one of the test datasets comprised of histopathology slides of an autoimmune disease, a condition with minimal data that has been underrepresented in medical imaging. In addition, our findings revealed that CASS is also more robust than the exiting state of the art self-supervised methods. The code is open source and is available on GitHub.

1 Introduction

In recent years, medical image analysis has seen tremendous growth due to the availability of powerful computational modelling tools, such as neural networks, and the advancement of techniques capable of learning from partial annotations. In this paper, we propose **Cross Architectural - Self Supervision (CASS)**, a novel self-supervised learning approach for learning useful data representations from limited samples of imagery sets.

Medical imaging is a field characterized by minimal data availability. First, data labelling typically requires domain-specific knowledge; therefore, the requirement of large-scale clinical supervision may be cost and time prohibitive. Second, due to patient privacy, disease prevalence, and other limitations, it is often difficult to release imaging datasets for secondary analysis, research, and diagnosis. Statistically, autoimmune diseases affect 3% of the US population or 9.9 million US citizens. On the other hand, 13.6 million (US citizens) or 4% of the US population, is affected by cancer. Cancer has been widely studied in medical science and at the intersection of medical

science and artificial intelligence. However, there are still major outstanding research questions for autoimmune diseases regarding the presence of different cell types and their role in inflammation at the tissue level. Their study is critical not only because they affect a large part of society but also because they have been on the rise recently Galeotti and Bayry [2020], Lerner et al. [2015], Ehrenfeld et al. [2020]. Other fields have benefited from the application of medical image analysis with the help of artificial intelligence. But for Autoimmune diseases, this is particularly challenging due to minimal data availability Tsakalidou et al. [2022], Stafford et al. [2020].

To overcome these limitations, we turn to self-supervised learning, that allows for learning in a label-free manner of useful data representations. Models extracting these representations can later be fine-tuned with a small amount of labelled data for each downstream task Sriram et al. [2021]. As a result, this learning approach avoids the relatively expensive and human-intensive task of data annotation and makes it an effective tool for the image analysis of emerging diseases that often have limited data availability (e.g., dermatomyositis, an autoimmune disease, or COVID-19, the cause of a recent worldwide pandemic). Existing approaches in the field of self-supervised learning purely rely either on Convolutional Neural Networks(CNNs) or Transformers as the feature extraction backbone and learn feature representations by teaching the network to compare the extracted representations. Instead, we propose to combine a CNN and Transformer in a response-based contrastive method. In CASS, the extracted representations of each input image is compared across two branches representing each architecture (see Figure 1). By transferring features sensitive to translation equivariance and locality from CNN to Transformer, CASS learns more predictive data representations in limited data scenarios where a Transformer-only model cannot find them. Our contributions are as follows:

- We introduce **Cross Architectural - Self Supervision (CASS)**, a hybrid CNN-Transformer approach for learning improved data representations in a self-supervised setting in limited data availability problems in the medical image analysis domain¹.
- We propose the use of CASS for analysis of autoimmune diseases such as dermatomyositis and demonstrate an improvement of 2.55% in comparison to the existing state of the art self-supervised approaches and 25% over supervised approaches for this problem.
- We evaluate CASS on three challenging medical image analysis problems (autoimmune disease cell classification, brain tumor classification, and skin lesion classification) on two public datasets (Brain tumor MRI Dataset Cheng [2017], Kang et al. [2021] and ISIC 2019 Tschandl et al. [2018], Gutman et al. [2018], Combalia et al. [2019]) and find that CASS outperforms existing state of the art self-supervised techniques by an average of 11.5% using 1% label fractions, 7.3 % with 10% label fractions and 8.5% with 100% label fractions.
- Existing methods also suffer a severe drop in performance when trained for a reduced number of epochs or batch size (Caron et al. [2021], Grill et al. [2020a], Chen et al. [2020a]). We show that CASS is robust to these changes in Appendix B and C.
- New state of the art self-supervised techniques are not only state of the art in terms of performance but also state of the art in terms of their computational requirements. This is a major hurdle as state of the art methods can take around 20 GPU days to train Azizi et al. [2021a]. This makes them inaccessible to someone with limited computational resources and increase triage in medical image analysis. CASS on average takes 69% less time as opposed to the existing state of the art method. We further expand on this result in Section 5.1 and further analyze this in Appendix D.

2 Background

2.1 Neural Network Architectures for Image Analysis

CNNs are a popular architecture of choice for many image analysis applications Khan et al. [2020]. CNNs learn more abstract visual concepts with a gradually increasing receptive field. They have two favorable inductive biases: (i) translation equivariance resulting in the ability to learn equally well with shifted object positions, and (ii) locality resulting in the ability to capture pixel-level closeness in the input data. CNNs have been used for many medical image analysis applications, such as disease diagnosis Yadav and Jadhav [2019] or semantic segmentation Ronneberger et al. [2015]. To address the requirement of additional context for a more holistic image understanding, the Vision Transformer (ViT) architecture Dosovitskiy et al. [2021] has been adapted to images from language-related tasks

¹The code is open source and available at: github.com/pranavsinghps1/CASS

and recently gained popularity Liu et al. [2021a, 2022a], Touvron et al. [2021]. In a ViT, the input image is split into patches, that are treated as tokens in a self-attention mechanism. In comparison to CNNs, ViTs can capture additional image context, but lack ingrained inductive biases of translation and location. As a result, ViTs typically outperform CNNs on larger datasets d’Ascoli et al. [2021].

ConViT d’Ascoli et al. [2021] combines CNNs and ViTs using gated positional self-attention (GPSA) to create a soft-convolution similar to inductive bias and improve upon the capabilities of Transformers alone. More recently, the training regimes and inferences from ViTs have been used to design a new family of convolutional architectures - ConvNext Liu et al. [2022b], outperforming benchmarks set by ViTs in classification tasks.

2.2 Self-Supervised Learning for Medical Imaging

Self-supervised learning allows for the learning of useful data representations without data labels Grill et al. [2020b], and is particularly attractive for medical image analysis applications where data labels are difficult to find Azizi et al. [2021a]. Recent developments have made it possible for self-supervised methods to match and improve upon existing supervised learning methods Hendrycks et al. [2019].

However, existing self-supervised techniques typically require large batch sizes and datasets. When these conditions are not met, a marked reduction in performance is demonstrated Caron et al. [2021], Chen et al. [2020a], Caron et al. [2020], Grill et al. [2020a]. Self-supervised learning approaches have been shown to be useful in big data medical applications Ghesu et al. [2022], Azizi et al. [2021b], such as analysis of dermatology and radiology imaging. In more limited data scenarios (3,662 images - 25,333 images), Matsoukas et al. [2021] reported that ViTs outperform their CNN counterparts when self-supervised pre-training is followed by supervised fine-tuning. Transfer learning favors ViTs when applying standard training protocols and settings. Their study included running the DINO Caron et al. [2021] self-supervised method over 300 epochs with a batch size of 256. However, questions remain about the accuracy and the efficiency of using existing self-supervised techniques when using them on datasets whose entire size is smaller than their peak performance batch size. Also, viewing this from the general practitioner’s perspective with limited computational power raises the question of how we can make practical self-supervised approaches more accessible? Adoption and faster development of self-supervised paradigms will only be possible when they become easy to plug-and-play with limited computational power.

In this work, we explore these questions by designing CASS, a novel approach developed with the core values of efficiency and effectiveness. In simple terms, we are combining CNN and Transformer in a response-based contrastive method by reducing similarity to combine the abilities of CNNs and Transformers. This approach was originally designed for a 198 image dataset for muscle biopsies of inflammatory lesions from patients who have dermatomyositis - an autoimmune disease. The benefits of this approach are illustrated by challenges in the diagnosis of autoimmune diseases due to their rarity, limited data availability, and heterogeneous features. As a result, misdiagnoses are common, and the resulting diagnostic delay plays a major factor in their high mortality rate. Autoimmune diseases also share commonalities with COVID-19 in terms of clinical manifestations, immune responses and pathogenic mechanisms. Moreover, some patients have developed autoimmune diseases after COVID-19 infection Liu et al. [2020]. Despite this increasing prevalence, the representation of autoimmune diseases in medical imaging and deep learning is limited. Furthermore, developing effective and efficient techniques such as CASS will aid in their widespread adoption, further expanding the work in multiple domains and resulting in a multifold improvement in quality of life.

Recent self-supervised methods define the inputs as two augmentations of one image and maximize the similarity between the two representations, by passing them through a pair of feature extractors. These feature extractors are similar in structure and only differ in their weights/parameters. Methods like Momentum Contrast (MoCo) He et al. [2020] and SiMCLR Chen et al. [2020b] maintain negative samples in a memory queue. The core idea in such scenarios is to bring the positive pairs together while repulsing the negative sample pairs. Recently, Bootstrap Your Own Latent (BYOL) Grill et al. [2020a] and DINO Caron et al. [2021] have improved upon this approach by eliminating the memory banks. The premise of using negative pairs is to avoid collapse. Several strategies have been developed with BYOL using a momentum encoder, Simple Siamese (SimSiam) Chen and He [2021] a stop gradient, and DINO applying the counterbalancing effects of sharpening and centering to avoid collapse. DINO is the first self-supervised training approach extended for Transformers. As described on the right side of Figure 1, DINO augments an image to produce two versions of the

image; these are then passed through the student and teacher networks, which are essentially the same encoder with different parameters. Their similarity is then measured with a cross-entropy loss. A stop-gradient (sg) operator is applied to the teacher network to propagate gradients only through the student network.

3 Methodology

We start by motivating our method before explaining in detail (in Section 3.1). Self-supervised methods until now have been using different augmentations of the same image. These were then passed through same architectures but with different set of parameters Grill et al. [2020a].

In Caron et al. [2021] they introduced crops of different sizes to add local and global information. They also used different operators and techniques to avoid collapse as described in Section 2.2.

Raghu et al. [2021] in their study suggested that for the same input, Transformers and CNNs extract different representations. They conducted their study by analyzing the CKA (Centered Kernel Alignment) for CNNs and Transformer using ResNet He et al. [2016] and ViT (Vision Transformer) Dosovitskiy et al. [2021] family of encoders. They found that Transformers have a more uniform representation across all layers as compared to CNNs. They also have self-attention, enabling global information aggregation from shallow layers and skip connections that connect lower layers to higher layers, promising information transfer. Hence, lower and higher layers in Transformers show much more similarity than in CNNs. The receptive field of lower layers for Transformers is more extensive than in CNNs. While this receptive field gradually grows for CNNs, it becomes global for Transformers around the midway point. Transformers don't attend locally in their earlier layers, while CNNs do. Using local information earlier is important for strong performance. CNNs have a more centered field as opposed to a more globally spread receptive field of Transformers. Hence, representations drawn from the same input, will be different for Transformers and CNNs. This inspired us to create positive pairs by different architectures or feature extractors rather than using different set of augmentations. This by design avoids collapse as the two architectures will never give the same representation as output. Furthermore, cross-architecture models have shown encouraging results for supervised-knowledge distillation as described in Gong et al. [2022].

3.1 Description of CASS

CASS' goal is to extract and then learn representations in a self-supervised way. To achieve this, an image is passed through a common set of augmentations. The augmented image is then passed through a CNN and Transformer to create positive pairs. The output logits from the CNN and Transformer are used to find cosine similarity loss (equation 1). Since, the two architectures give different representations as mentioned in Raghu et al. [2021], the model doesn't collapse. We also report results for CASS using different set of CNNs and Transformers in Appendix B and C, and not a single case of model collapse was found.

$$\text{loss} = 2 - 2 \times \left(\sum_{i=1}^N \left(\frac{R}{(\max \|R\|_2, \epsilon)} \right) \right) \times \left(\sum_{i=1}^N \left(\frac{T}{(\max (\|T\|_2, \epsilon)} \right) \right) \quad (1)$$

We use same parameters for optimizer and learning schedule for both the architectures. We also use stochastic weight averaging (SWA) Izmailov et al. [2018] with Adam optimizer and a learning rate of 1e-3. For learning rate we use cosine schedule with a maximum of 16 iterations and a minimum value of 1e-6. ResNets are typically trained with Stochastic Gradient Descent (SGD) and our use of Adam optimizer is quite unconventional.

In figure 1, we show CASS on left side and DINO Caron et al. [2021] on the right. Comparing the two, CASS drops a lot of extra mathematical treatment used in DINO to avoid collapse such as centring and applying softmax function on the output of its student and teacher networks. After training CASS and DINO for one cycle, DINO yields only one kind of trained architecture, while CASS provides two trained architectures (1 - CNN and 1 - Transformer). CASS trained architectures provide better performance than DINO trained architectures in most cases as further elaborated in Section 5.

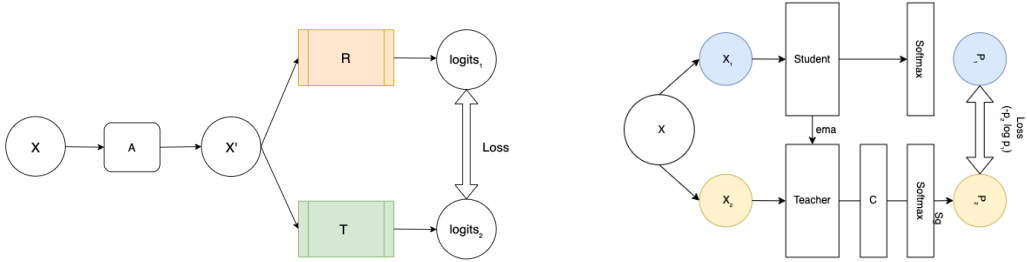


Figure 1: (left) In our proposed self-supervised architecture - CASS, R represents ResNet-50, a CNN and T in the other box represents the Transformer used (ViT); X is the input image, which becomes X' after applying augmentations. Note that CASS applies only one set of augmentations to create X' . X' is then passed through both the arms to compute loss as mentioned in Equation 1. This is different from DINO mentioned on the right, which passes different augmentation of the same image through networks with the same architecture but different parameters. The output of the teacher network is centred on a mean computed over a batch. Another key difference is that in CASS, loss is computed over logits meanwhile in DINO it is computed over softmax output.

4 Experimental Details

4.1 Self-supervised learning

We studied and compared results between DINO and CASS trained self-supervised CNNs and Transformers. For the same, we trained from ImageNet initialization for 100 epochs with a batch size of 16. We ran these experiments on an internal cluster with single GPU unit (NVIDIA RTX8000) with 48 GB video RAM, 2 CPU cores and 64 GB system RAM.

For DINO, we used the hyper parameters and augmentations mentioned in the original implementation.

For CASS, we describe the experimentation details in Appendix E.

4.2 Linear Fine-tuning

Following the linear evaluation protocol as specified in Chen et al. [2020b], we froze the model after self-supervised training, and trained a linear classifier on top of it. The test set metrics were used as proxies for representation quality. We trained the classifier for a maximum of 50 epochs with an early stopping patience of 5 epochs. For supervised fine tuning we used Adam optimizer with a cosine annealing learning rate starting at $3e-04$. Since almost all medical datasets have some class imbalance we applied class distribution normalized Focal Loss Lin et al. [2017] to navigate class imbalance.

4.3 Datasets

We compared supervised and self-supervised models (DINO versus CASS) over three datasets of different modalities. We applied general splitting strategy of 80/10/10 for training/validation and testing unless mentioned otherwise. All images were resized to 384 square images, unless mentioned otherwise. We also provide some samples from the datasets used to give an idea about the modalities.

- **Autoimmune diseases biopsy slides** (Van Buren et al. [2022]) consists of slides cut from muscle biopsies of dermatomyositis patients stained with different proteins and imaged to generate a dataset of 198 TIFF image set from 7 patients. The presence or absence of these cells helps to diagnose dermatomyositis. Multiple cell classes can be present per image; therefore this is a multi-label classification problem. Our task here was to classify cells based on their protein staining into TFH-1, TFH-217, TFH-Like, B cells, and others. We used F1 score as our metric for evaluation, as employed in the original work by Van Buren et al. [2022]. These RGB images have a consistent size 352 by 469.
- **Brain tumor MRI dataset** Cheng [2017], Amin et al. [2022] 7022 images of human brain MRI images that are classified into four classes: glioma, meningioma, no tumor, and pituitary.

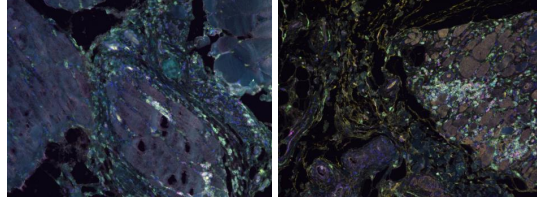


Figure 2: Sample of autofluorescence slide images from the muscle biopsy of patients with dermatomyositis - a type of autoimmune disease.

We used the dataset from <https://www.kaggle.com/datasets/masoudnickparvar/brain-tumor-mri-dataset> that combines Br35H: Brain tumor Detection 2020 dataset used in "Retrieval of Brain tumors by Adaptive Spatial Pooling and Fisher Vector Representation" and Brain tumor classification curated by Navoneel Chakrabarty and Swati Kanchan. Out of these, the dataset curator created the training and testing splits. We followed their splits, 5,712 images for training and 1,310 for testing. This dataset is relatively balanced. Since this was a combination of multiple datasets, size of images vary throughout the dataset. The pretext of the task is multi-class classification, and we used the F1 score as the metric. Since, the dataset we used is a combination of multiple datasets, image sizes vary from 512×512 to 219×234.

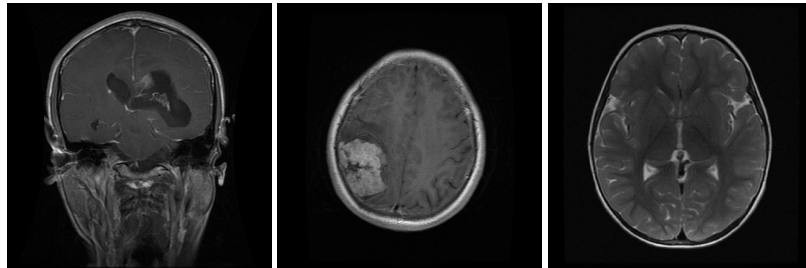


Figure 3: Sample images of brain tumor MRI dataset, Each image corresponds to a prediction class in the data set glioma (Left), meningioma (Center) and No tumor (Right)

- **ISIC 2019** (Tschandl et al. [2018], Gutman et al. [2018], Combalia et al. [2019]) consists of 25,331 images across eight different categories - melanoma (MEL), melanocytic nevus (NV), Basal cell carcinoma (BCC), actinic keratosis(AK), benign keratosis(BKL) , dermatofibroma(DF), vascular lesion (VASC) and Squamous cell carcinoma(SCC). This dataset contains images of size 600×450 and 1024×1024 . The distribution of these labels is unbalanced across different classes. For evaluation, we followed the metric followed in the official competition i.e balanced multi-class accuracy value, which is semantically equal to recall. We further expand on this dataset in Appendix D.



Figure 4: Sample images from the ISIC-2019 challenge dataset.

5 Results and Discussion

5.1 Compute and Time analysis Analysis

We ran all the experiments on a single NVIDIA RTX8000 GPU with 48GB video memory. In Table 2, we compare the cumulative training times for self-supervised training of a CNN and Transformer with DINO and CASS. We observed that CASS took an average of 69% less time compared to DINO. Another point to note is that, CASS trained two architectures at the same time or in a single pass. While to train a CNN and Transformer with DINO it would take two separate passes.

Table 1: Self-supervised training comparison for 100 epochs on a Single RTX8000 GPU.

Dataset	DINO	CASS
Autoimmune	1 Hour 13 Mins	21 Mins
Brain MRI	26 Hours 21 Mins	7 Hours 11 Mins
ISIC-2019	109 Hours 21 Mins	29 Hours 58 Mins

5.2 Autoimmune Diseases Biopsy Slides Dataset

We did not perform 1% training for the autoimmune diseases biopsy slides of 198 images because using 1% images would be too small number to learn anything meaningful and the results would be highly randomized.

Following the self-supervised training and fine tuning procedure as described in Section 4.1 and 4.2, we observed that using CASS with the ViT B/16 backbone and ResNet50 improved upon existing result of 0.63 Van Buren et al. [2022] to 0.8894. All kinds of Transformers consistently outperformed CNNs. This finding was explained by the information spread throughout the image, instead of localized in a single spot (See Figure 2).

Table 2: Results for autoimmune biopsy slides dataset. In this table we compare the F1 score on test set. We observed that CASS outperformed the existing state-of-art self-supervised method using 100% labels for CNN as well as for Transformers. Although DINO outperforms CASS for CNN for 10% labelled fraction. Overall CASS outperforms DINO by 2.2% for 100% labelled training for CNN and transformer. For Transformers in 10% labelled training CASS performance was 2.7% better than DINO.

Techniques	Backbone	Testing F1 score	
		10%	100%
DINO	Resnet-50	0.8237±0.001	0.84252±0.008
CASS	Resnet-50	0.8158±0.0055	0.8650±0.0001
Supervised	Resnet-50	0.82095±0.007	0.819±0.0216
DINO	ViT B/16	0.8445±0.0008	0.8639± 0.002
CASS	ViT B/16	0.8717±0.005	0.8894±0.005
Supervised	ViT B/16	0.8356±0.007	0.8420±0.009

5.3 Brain tumor MRI dataset

We observed that supervised CNNs performed better than Transformers on this dataset. Similarly, for DINO CNNs performed better than Transformers by a margin. We observed that this trend is followed by CASS as well. The difference between CNN and Transformer performance is smaller for CASS as compared to the difference in performance for CNN and Transformer with supervised or DINO training. We report these results in Table 3. We further discuss these results in Appendix D.

5.4 ISIC 2019 Dataset

The ISIC-2019 dataset is an incredibly challenging dataset, not only because of the class imbalance issue but because it is made of partially processed and inconsistent images with hard-to-classify

Table 3: The brain tumor MRI dataset results followed the same trend as in Table 1. While DINO out performed CASS for 1% and 10% labelled training for CNN, CASS maintained its superiority for 100% labelled training, albeit by just 0.09%. Similarly, CASS outperformed DINO for all data regimes for transformers, incrementally 1.34% in for 1%, 3.04% for 10% and 4.38% for 100% labelled training. We observe that this margin is more significant than for biopsy images. Such results could be ascribed to the increase in dataset size resulting in an increase in learnable information.

Techniques	Backbone	Testing F1 score		
		1%	10%	100%
DINO	Resnet-50	0.63405±0.09	0.92325±0.02819	0.9900±0.0058
CASS	Resnet-50	0.40816±0.13	0.8925±0.0254	0.9909± 0.0032
Supervised	Resnet-50	0.52±0.018	0.9022±0.011	0.9899± 0.003
DINO	ViT B/16	0.3211±0.071	0.7529±0.044	0.8841± 0.0052
CASS	ViT B/16	0.3345±0.11	0.7833±0.0259	0.9279± 0.0213
Supervised	ViT B/16	0.3717 ± 0.077	0.787±0.0245	0.9419± 0.017

classes. We further expand on this in Appendix D. From Table 4 it is clear that CASS outperforms DINO for all label fractions for both CNN and Transformer by a margin.

Table 4: Results for the ISIC-2019 dataset. Comparable to the official metrics used in the challenge <https://challenge.isic-archive.com/landing/2019/>. We use balanced multi-class accuracy as our metric, which is semantically equal to recall value. We observe that some results are inconsistent with an increase in label fraction; we discuss this curious case in Appendix D. Overall, CASS consistently improved upon existing methods for all label fractions.

Techniques	Backbone	Testing Balanced multi-class accuracy		
		1%	10%	100%
DINO	Resnet-50	0.518±3.9e-08	0.3197±0.0027	0.3597±0.0027
CASS	Resnet-50	0.5217±1.6e-06	0.5802±0.00119	0.5209±2.85e-05
Supervised	Resnet-50	0.2640±0.031	0.3070±0.0121	0.35±0.006
DINO	ViT B/16	0.3183± 0.1338	0.3646±0.0765	0.3908±0.001
CASS	ViT B/16	0.7258± 0.0465	0.6195±0.0179	0.6519±0.001
Supervised	ViT B/16	0.4436±0.007	0.3097±0.0314	0.3279±0.007

5.5 Ablation Studies

5.5.1 Change in batch size

To gauge the change in performance with the change in batch size, we ran experiments with CASS with a batch size of 8, 16, and 32. We present these results in Appendix B and C. Based on them we concluded that CASS is robust to batch size changes. Interestingly, instead of dropping performance like existing methods, CASS-trained Transformers with smaller batch sizes performed better.

5.5.2 Training Epochs

We report the performance of CASS trained for 50, 100, 200 and 300 epochs in Appendix B and C. On reducing the epochs to 50, a performance drop of 2% was observed for CNN, while the performance of Transformer remained almost the constant. Similarly, there is a 2% gain when we double the number of self-supervised training epochs. However, after that, the gain is minimal from 200 to 300.

5.5.3 Effect of augmentation change

CASS does not use hard augmentations like DINO or BYOL. We study the effect of adding BYOL/DINO-like augmentations in Appendix B. Although, Gaussian blur helps in converging the CNN and Transformer for CASS. We find that adding BYOL-like hard augmentations costs

performance. CASS has global-local cropping inbuilt due to difference in the receptive field of CNN and Transformers, unlike DINO, where it was added.

5.5.4 Change in architecture

We provide intuition for changing the architecture of CNNs and Transformers in Appendix B and C. As a baseline we started with ResNet-50 and ViT Base/16 Transformer for our experiments. But we also expand these results to other CNN and Transformer families. Furthermore, we also report results of using two CNNs or two Transformers on the brain MRI classification dataset in Appendix C.

5.6 Optimization

For CASS, we used Adam optimizer for both CNN and Transformer. Traditionally, CNNs and more specifically ResNets have been used with a SGD optimizer, but in our case we use Adam optimiser. This choice is fairly unconventional and expand upon this in Appendix B.

5.7 Initialization

We use ImageNet initialized CNN and Transformers for CASS, DINO and supervised training. Use Timm’s library for these initialization Wightman [2019]. ImageNet initialization is preferred for transfer learning in medical image analysis not because of feature reuse but because ImageNet weights allow for faster convergence through better weight scaling Raghu et al. [2019]. But sometimes pretrained weights might be hard to find, so we study CASS’ performance with random and ImageNet initialization in Appendix C.4.

5.8 Limitations

Although CASS performance for larger and non-biological data can be hypothesized based on inferences, a complete study on large-sized natural datasets hasn’t been conducted. In this study, we focused extensively on studying the effects and performance of our proposed method for small batch sizes and limited computational resources. In a low-data regime, CASS trained CNN performed worse than existing methods on datasets with centrally localized information images, if applied without making correct changes.

6 Potential negative societal impact

The autoimmune dataset is limited to a geographic institution. Hence the study is specific to a disease variant. Inferences drawn may or may not hold true for other variants. Also, the results produced are dependent on a set of markers. Medical practitioners often require multiple tests before finalising diagnosis; medical history and existing health conditions also play an essential role. We haven’t incorporated the aforementioned meta-data in CASS.

Neglecting the tendencies and biases of the dataset under consideration, could even lead the state-of-the-art model to underperform. Hence jeopardizing trust for computer based methods in medical imaging. Finally, application on a wider scale - real life scenarios should only be trusted after taking clearance from the concerned health and safety governing bodies.

7 Conclusion

Self-supervised learning is important for medical image analysis, but existing methods require a lot of computational power. Based on our experimentation on three diverse medical imaging datasets, we empirically conclude that CASS gained an average of 8.5% with 100% labelled data, 7.3% with 10% labelled data, and 11.5% with 1% labelled data and trained in 69% less time as opposed to the existing state of the art self-supervised method. Furthermore, we saw that CASS is robust to change in batch size (Appendix B.1 and C.2), reduction in training epochs (Appendix B.2 and C.3) and change in initialization (Appendix C.4).

CASS is 69% computationally efficient while also delivering better performance and more robustness than the existing state of the art methods. This ease of accessibility and better performance will

catalyze medical imaging research to help us improve healthcare solutions as well as develop new solutions for underrepresented and emerging diseases.

A Self-supervised Algorithm

The core self-supervised algorithm, used to train CASS with a CNN (R) and a Transformer (T), is described as follows for one epoch:

Algorithm 1: Herein we describe CASS self-supervised training algorithm

Input: Unlabeled same augmented images from the training set x'
Output: Logits from each network.
Data: Images from a given dataset

```

1 for x in train loader: do
2     R = cnn(x') // taking logits output from CNN
3     T = vit(x') // taking logits output from ViT
4     loss = 2 - 2* (sum_{i=1}^N (R / (max(||R||_2), epsilon)) * sum_{i=1}^N (T / (max(||T||_2), epsilon))) // taking cosine
5     similarity between the logits outputs from CNN and ViT
6     Calculate the mean value of all elements of the loss tensor.
7     Compute gradients.

```

B Ablation Study

B.1 Batch size

We used 16 as our standard batch size. As mentioned already with CASS we aim to overcome the shortcomings of existing self-supervised methods where they drop a lot of performance with reduction in batch size. To study this effect, we ran CASS with three different batch sizes on the autoimmune dataset - 8, 16 and 32. We follow the standard set of protocols as mentioned in Appendix E for training. We also conducted this experiment on the brain MRI classification dataset and report the results in Appendix C.2.

Batch Size	CNN F1 Score	Transformer F1 Score
8	0.88285±0.0011	0.8744±0.0009
16	0.8650±0.0001	0.8894±0.005
32	0.8648±0.0005	0.889±0.0064

Table 5: F1 metric comparison between the two arms of CASS trained over 100 epochs, following the protocols and procedure listed in Appendix E. We only change the batch size during self-supervised training. Based on these we observed that while CASS trained Transformer gains 1% with reduction in batch size from 16 to 8, CASS trained CNN gains almost 2% for the same change. Although there is a diminishing gain in performance as we increase the batch size.

B.2 Change in training epochs

As standard we trained CASS for 100 epochs in all cases. But existing self-supervised techniques are plagued with a loss in performance with a decrease in number of training epochs. To test this effect for CASS, we run it for 50, 100, 200 and 300 epochs on the autoimmune dataset and report the results in Table 6. Additionally, we also ran the same experiment on the brain MRI dataset and report the results in Appendix C.3.

B.3 Augmentations

Contrastive learning techniques are known to be extremely dependent on augmentations. Recently, most of the self-supervised techniques have adopted BYOL Grill et al. [2020a]-like set of augmen-

Epochs	CNN F1 Score	Transformer F1 Score
50	0.8521 \pm 0.0007	0.8765 \pm 0.0021
100	0.8650 \pm 0.0001	0.8894 \pm 0.005
200	0.8766 \pm 0.001	0.9053 \pm 0.008
300	0.8777 \pm 0.004	0.9091 \pm 8.2e-5

Table 6: Performance comparison over varied number of epochs, from 50 to 300 epochs, the downstream training procedure and the CNN-Transformer combination is kept constant across all the four experiments, only the number of self-supervised epochs have been changed.

tations. DINO Caron et al. [2021] uses the same set of augmentations as BYOL, along with the addition of a local-global cropping. For CASS, we use a reduced set of BYOL augmentations, along with a few changes. For instance we don't use solarize and Gaussian blur. Instead we use affine transformations and random perspective. In this section we study the effect of adding BYOL-like augmentations to CASS. We report these results in Table 7.

Augmentation Set	CNN F1 Score	Transformer F1 Score
CASS only	0.8650 \pm 0.0001	0.8894 \pm 0.005
CASS + Solarize	0.8551 \pm 0.0004	0.81455 \pm 0.002
CASS + Gaussian blur	0.864 \pm 4.2e-05	0.8604 \pm 0.0029
CASS + Gaussian blur + Solarize	0.8573 \pm 2.59e-05	0.8513 \pm 0.0066

Table 7: We report the F1 metric of CASS trained with different set of augmentations for 100 epochs. We provide an extensive list of augmentations used for CASS in detail in section C.2.2.

We observe that while CASS trained CNN fluctuates within a percent of its peak performance, CASS trained Transformer drops performance with the addition of solarization and Gaussian blur. Interestingly, the two arms converged with the use of Gaussian blur.

B.4 Optimization

In CASS we use Adam optimizer for both CNN and Transformer. This is a shift from the traditional use of SGD or stochastic gradient descent for CNNs. In this Table 8 we report the performance of CASS trained CNN and Transformer while CNN using SGD and Adam optimizer.

Optimiser for CNN	CNN F1 Score	Transformer F1 Score
Adam	0.8650 \pm 0.0001	0.8894 \pm 0.005
SGD	0.8648 \pm 0.0005	0.82355 \pm 0.0064

Table 8: We report the F1 metric of CASS trained with different set of optimizers for the CNN arm for 100 epochs. We observe that while there is no change in performance of the CNN, the performance of the Transformer drops quite a bit with the use of SGD.

B.5 Change in architecture

B.5.1 Changing Transformer and keeping the CNN same

CNN	Transformer	CNN F1 Score	Transformer F1 Score
ResNet-50	ViT Base/16 (86.86M)	0.8650 \pm 0.001	0.8894 \pm 0.005
	ViT Large/16 (304.72M)	0.8481 \pm 0.001	0.853 \pm 0.004

Table 9: Simply increasing the model size or choosing on the basis of ImageNet performance wouldn't lead better results. As mentioned already in Section 6, it is important to understand the biases and tendencies of a dataset to extract maximum performance.

Architecture	Testing F1 Score
ResnNet-50	0.819 \pm 0.0216
ViT Base/16	0.8420 \pm 0.009
ViT large/16	0.80495 \pm 0.0077

Table 10: Supervised performance of ViT family on the autoimmune dataset. We observed that as opposed to ImageNet performance ViT large/16 performs worse than ViT Base/16 on the autoimmune dataset.

From Table 9 and 10 we observed that CASS trained ViT Transformer with the same CNN, consistently gained approximately 4.7% over its supervised counterpart. We also report results on the brain MRI classification dataset in Appendix C.1.2.

B.5.2 Changing CNN and keeping the Transformer same

CNN	Transformer	100% Label Fraction	
		CNN F1 score	Transformer F1 score
ResNet-18 (11.69M)		0.8674 \pm 4.8e-5	0.8773 \pm 5.29e-5
ResNet-50 (25.56M)	ViT Base/16 (86.86M)	0.8650 \pm 0.001	0.8894 \pm 0.0005
ResNet-200 (64.69M)		0.8517 \pm 0.0009	0.874 \pm 0.0006

Table 11: F1 metric comparison between the two arms of CASS trained over 100 epochs, following the protocols and procedure listed in Appendix E. The numbers in parentheses show the parameters learned by the network. We use Wightman [2019] implementation of CNN and transformers, with ImageNet initialisation.

Architecture	Testing F1 Score
ResnNet-18	0.8299 \pm 0.0004
ResnNet-50	0.819 \pm 0.0216
ResnNet-200	0.833 \pm 0.0005

Table 12: Supervised performance of the ResNet CNN family on the autoimmune dataset. Similar to Table 6, the results for supervised CNNs don't follow ImageNet trend.

From Table 9, 10, 11 and 12 we can conclude that for a given dataset, it is better to use check supervised performance and then combine in CASS, to extract maximum performance available for the dataset.

C Additional Results

We conducted some further experimentation to check for collapse and for ablation studies. The model did not report collapse in any case. The following results are calculated following the protocols in Appendix E on the brain MRI classification dataset.

C.1 Effect of Changing the ViT/CNN branch

C.1.1 Changing CNN while keeping Transformer same

For this experiment we use ResNet family of CNNs along with ViT base/16 as our Transformer. We observed that the performance of Transformer increases with increase in the difference between the size of CNN and Transformer. The performance of CNN remains almost same in all three cases. We present these results in Table 13.

CNN	Transformer	100% Label Fraction	
		CNN F1 score	Transformer F1 score
ResNet-18 (11.69M)		0.9913 \pm 0.002	0.9801 \pm 0.007
ResNet-50 (25.56M)	ViT Base/16 (86.86M)	0.9909 \pm 0.0032	0.9279 \pm 0.0213
ResNet-200 (64.69M)		0.9898 \pm 0.005	0.9276 \pm 0.017

Table 13: F1 metric comparison between the two arms of CASS trained over 100 epochs, following the protocols and procedure listed in Appendix B. The numbers in parentheses show the parameters learned by the network. We use Wightman [2019] implementation of CNN and transformers, with ImageNet initialisation.

C.1.2 Changing Transformer while keeping CNN same

For this experiment we keep the CNN as constant and study the effect of changing the Transformer. For this experiment we use ResNet as our choice of CNN and ViT base and large Transformers with 16 patches. Additionally we also report performance for DeiT-B with ResNet-50. We report these results in Table 14.

CNN	Transformer	CNN F1 Score	Transformer F1 Score
ResNet-50 (25.56M)	ViT Base/16 (86.86M)	0.9909 \pm 0.0032	0.9279 \pm 0.0213
	ViT Large/16 (304.72M)	0.98945 \pm 2.45e-5	0.8896 \pm 0.0009
	DeiT Base/16 (86.86M)	0.989 \pm 0.0025	0.9844 \pm 0.0048

Table 14: For the same number of Transformer parameters, DeiT-base with ResNet-50 performed much better than ResNet-50 with ViT-base. The difference in their CNN arm is 0.10%. On ImageNet DEiT-base has a top1% accuracy of 83.106 while ViT-base has an accuracy of 86.006. We use both the Transformers with 16 patches. [ResNet-50 has an accuracy of 80.374]

Hence, it could be seen that for a constant architecture in one arm, the better choice of architecture in the second arm would be the one with worse ImageNet performance. This could also be identified from the table above where Transformer performed the best with the CNN which performed the worse on ImageNet.

C.1.3 Using CNN in both arms

Until now we have experimented by using a CNN and a Transformer in CASS. In this section we present results for using two CNNs in CASS. We pair ResNet-50 with DenseNet-161. We observe that both the CNNs fail to reach the benchmark set by ResNet-50 and ViT-B/16 combination. Although training the ResNet-50-DenseNet-161 pair takes 5 hour 24 minutes which is less than the 7 hours 11 minutes taken by the ResNet-50-ViT-B/16 combination to be trained with CASS.

CNN	Architecture in the other arm	F1 Score of ResNet-50 arm	F1 Score of the other arm
ResNet-50	ViT Base/16 DenseNet-161	0.9909 \pm 0.0032 0.9743 \pm 8.8e-5	0.9279 \pm 0.0213 0.98365 \pm 9.63e-5

C.1.4 Using Transformer in both arms

Similar, to the above section, for this section we use a Transformer-Transformer combination instead of a CNN-Transformer combination. For this we use Swin-Transformer patch-4/window-12 Liu et al. [2021b] alongside ViT-B/16 Transformer. We observe that the performance for ViT-B/16 improves by around 1.3% when we use Swin Transformer. Although this comes at computational cost. Swin-ViT combination took 10 hours to train as opposed to 7 hours 11 minutes taken by the ResNet-50-ViT-B/16 combination to be trained with CASS. Even with the increase in time taken to train the Swin-ViT combination, it is still almost 50% less than DINO. We present these results in Table 15.

Architecture in the other arm	Transfomer	F1 Score	F1 Score of ViT-B/16 arm
ResNet-50	ViT Base/16	0.9909 \pm 0.0032	0.9279 \pm 0.0213
Swin Tranformer		0.9883 \pm 1.26e-5	0.94 \pm 8.12e-5

Table 15: We present the results for using Transformers in both the arms and compare the results with CNN-Transformer combination.

C.2 Changing Batch Size

This section presents results of varying the batch size in the brain MRI classification dataset. In the standard implementation of CASS, we used a batch size of 16; here, we additionally showed results for batch sizes 8 and 32. The largest batch size we could run was 34 on a single GPU of 48 GB video memory. Hence 32 was the biggest batch size we showed in our results. Although the performance of CNN remained nearly constant with a change of less than a percentage over the three datasets. The performance of the Transformer drops as we increase the batch size. Since CASS was developed with the requirements of running on small datasets, with an overall size smaller than the batch size of current state of the art techniques, its peak performance for small batch size justifies the rationale for its development.

From Table 5 and 16, we observed that reduction in batch size increase CASS performance. Also, the fluctuation in performance wasnt a lot, hence cementing its robustness to change in batch size.

Batch Size	CNN F1 Score	Transformer F1 Score
8	0.9895 \pm 0.0025	0.93158 \pm 0.0109
16	0.9909 \pm 0.0032	0.9279 \pm 0.0213
32	0.9848 \pm 0.011	0.9176 \pm 0.006

Table 16: We observe a small gain for CNN with moderate batch size, performance for the transformer improves as we reduce the batch size. We maintain the downstream batch size constant for all the three self-supervised batch sizes, following the standard experimental setup as mentioned in Appendix E. These results are for 100% label fraction.

C.3 Effect of the Number of Training Epochs

We saw that there was an incremental gain in performance as we increased the number of self-supervised training epochs. For the opposite scenario, there wasn't a steep drop in performance like the existing self-supervised techniques when we reduce the number of self-supervised epochs. Table 12 displays results for this experimentation.

Self-supervised training epochs	CNN F1 Score	Transformer F1 Score
50	0.9795 \pm 0.0109	0.9262 \pm 0.0181
100	0.9909 \pm 0.0032	0.9279 \pm 0.0213
200	0.9864 \pm 0.008	0.9476 \pm 0.0012
300	0.9920 \pm 0.001	0.9484 \pm 0.017

Table 17: Performance comparison over varied number of epochs, from 50 to 300 epochs, the downstream training procedure and the CNN-transformer combination is kept constant across all the four experiments, only the number of self-supervised epochs has been changed.

From Table 2 and 12, we observe that changing the training epochs reports the same effect for both the datasets.

C.4 Effect of Initialization

We observed that performance almost remained the same with minor gains when the initialization was altered for the two networks. Table 18 presents the results for this experimentation.

	Initialisation	CNN F1 Score	Transformer F1 Score
Random		0.9907 ± 0.009	0.9316 ± 0.027
Imagenet		0.9909 ± 0.0032	0.9279 ± 0.0213

Table 18: We observe that the Transformer gains some performance with random initialization, although performance has more variance when used with random initialization.

D Result Analysis

D.1 Time complexity analysis

In section 5.1, we observed that CASS takes 69% less time as compared to DINO. This reduction in time could be attributed to the following reasons:

1. In DINO, augmentations are applied twice as opposed to just once in CASS. Furthermore, we per application CASS uses less number of augmentations as compared to DINO.
2. Since the architectures, used are different, there is no scope of parameter sharing between them. A major chunk of time is saved in just updating the two architectures, after each epoch instead of re-initializing architectures with lagging parameters.

D.2 Comparison of Performance

In Table 14, we report the best-performing model from Resnet-50/ViT B/16 for CASS, DINO, and supervised training. We found that CASS consistently outperformed supervised learning across all data regimes for two datasets. For the brain MRI dataset, CASS was comparable to supervised learning for 10% and 100% label fractions, while it had gained performance for 1% label fraction.

Compared to the existing State of the art self-supervised method, DINO - we observed that CASS matched or outperformed DINO in the 100% data regime consistently. We present a more in-depth discussion on these results in Section 5, Appendix D.3 and D.4.

Table 19: Comparison of best performing models across CASS, DINO and supervised learning methods on three datasets with different levels of supervision. We chose not to run 1% label fraction experiment for the autoimmune dataset, since it only has 198 images, and fine tuning would have negligible and very varied effect. Instead we ran these models with different seeds, and present averaged results over 5 runs in this table.

Dataset	Regime	CASS	DINO	Supervised	Metric
Autoimmune	10%	0.8717 ± 0.005	0.8445 ± 0.0008	0.8356 ± 0.007	F1 Score
	100%	0.8894 ± 0.005	0.8639 ± 0.002	0.8420 ± 0.009	
Brain MRI	1%	0.40816 ± 0.13	0.63405 ± 0.09	0.3717 ± 0.077	F1 Score
	10%	0.8925 ± 0.0254	0.92325 ± 0.02819	0.9022 ± 0.011	
	100%	0.9909 ± 0.0058	0.9900 ± 0.0032	0.9899 ± 0.003	
ISIC 2019	1%	0.7258 ± 0.0465	$0.518 \pm 3.9e-08$	0.52 ± 0.018	Balanced
	10%	0.6195 ± 0.0179	0.3646 ± 0.0765	0.3097 ± 0.0314	Multi-Class Accuracy
	100%	0.6519 ± 0.001	0.3908 ± 0.001	0.35 ± 0.006	

D.3 Brain MRI classification

Many images in the brain tumor MRI dataset have most of the data center-localized, with blank padding around the central part. To address such cases, a better approach is to use center crop to guide the model to learn desirable attributes. But this is a mixed dataset i.e it contains images of different dimensions, so using center crop with resizing would not yield consistent results. For this study, we did not make any changes to augmentations of the models and followed standard training procedures. From Raghu et al. [2021] we learned that CNN’s receptive field was much more intense

and centered. Hence, CNNs were only able to pay attention to the informative center part in most images. This finding was empirically validated by our results, with purely CNN-based supervised and self-supervised technique (DINO) performing much better than purely Transformer based supervised and self-supervised technique (DINO) across the board. Comparing only the CNN component, CASS with its CNN/Transformer combination struggled in low data-regime as compared to purely-CNN based training approaches but slightly outperformed with 100% labels.

On comparing the Transformer component, CASS consistently outperformed purely Transformer supervised and self-supervised counterparts across all data regimes. The gains were in proportion to the percentage of labels used.

D.4 Curious case of ISIC 2019 dataset

ISIC 2019 consists of images from the HAM10000 and BCN_20000 datasets Cassidy et al. [2022], Gessert et al. [2020]. For the HAM1000 dataset, it is difficult to classify between 4 classes (melanoma and melanocytic nevus), (actinic keratosis and benign keratosis). HAM10000 dataset contains images of size 600×450 , centred and cropped around the lesion. Histogram corrections have been applied to only a few images. Similarly, the BCN_20000 dataset contains images of size 1024×1024 . This dataset is particularly challenging as many images are uncropped, and lesions are in difficult and uncommon locations. Overall this dataset is highly unbalanced, with almost 50% or 12,875 (out of 25,331) samples of Melanocytic nevus. Melanoma and melanocytic nevus are hard to distinguish from each other. Melanocytic nevus has 12,875 (out of 25,331) samples while melanoma has only 4,522, i.e. Melanocytic nevus has three times the melanoma sample. Similarly, actinic keratosis and benign keratosis are hard to distinguish. There are almost four times more benign keratosis samples than actinic keratosis. Furthermore, class distribution changes whenever we randomly sample from the dataset. This change in distribution throws off the focal loss, which uses class weights based on the overall class distribution of the dataset. Altogether, these might contribute to the erratic behaviour of all three models in some cases.

E In-detail experimentation details

E.1 Self-supervised training

E.1.1 Protocols

- Self-supervised learning was only done on the training data and not on the validation data. We used <https://github.com/PyTorchLightning/pytorch-lightning> to set the pseudo-random number generators in PyTorch, NumPy and (python.random).
- We run training over five different seed values, and report mean results with variance in each table. We don't perform a seed value sweep to extract anymore performance Picard [2021].
- For DINO implementation we use Phil Wang's implementation: <https://github.com/lucidrains/vit-pytorch>.
- For implementation of CNNs and Transformers we use timm's library Wightman [2019].
- For all experiments, ImageNet Deng et al. [2009] initialised CNN and Transformers were used.

E.1.2 Augmentations

- Resizing: Resize input images to 384X384 with bilinear interpolation.
- Color jittering: change the brightness, contrast, saturation and hue of an image or apply random perspective with a given probability. We set the degree of distortion to 0.2 (between 0 and 1) and use bilinear interpolation, with an application probability of 0.3.
- Color jittering or apply random affine transformation of the image keeping center invariant with degree 10, with an application probability of 0.3.
- Horizontal and Vertical flip. Each with an application probability of 0.3.
- Channel normalisation with mean (0.485, 0.456, 0.406) and standard deviation (0.229, 0.224, 0.225).

E.1.3 Hyper-parameters

- Optimization: We use stochastic weighted averaging over Adam optimiser with learning rate (LR) set to 1e-3 for both CNN and vision transformer (ViT). This is a shift from SGD which is usually used for CNNs.
- Learning Rate: Cosine annealing learning rate is used with 16 iterations and a minimum learning rate of 1e-6. Unless mentioned otherwise, this setup was trained over 100 epochs. These were then used as initialisation for the downstream supervised learning. The standard batch size is 16.

E.2 Supervised training

E.2.1 Augmentations

We use the same set of augmentations used in self-supervised training.

E.2.2 Hyper-parameters

- We use Adam optimiser with lr set to 3e-4 and a cosine annealing learning schedule.
- Since, all medical datasets have class imbalance we address it by using focal loss Lin et al. [2017] as our choice of loss function with the alpha value set to 1 and the gamma value to 2. In our case it uses minimum-maximum normalised class distribution as class weights for focal loss.
- We train for 50 epochs. We also use a five epoch patience on validation loss to check for early stopping. This downstream supervised learning setup is kept the same for CNN and Transformers.

References

Caroline Galeotti and Jagadeesh Bayry. Autoimmune and inflammatory diseases following covid-19. *Nature Reviews Rheumatology*, 16(8):413–414, 2020.

Aaron Lerner, Patricia Jeremias, and Torsten Matthias. The world incidence and prevalence of autoimmune diseases is increasing. *Int J Celiac Dis*, 3(4):151–5, 2015.

Michael Ehrenfeld, Angela Tincani, Laura Andreoli, Marco Cattalini, Assaf Greenbaum, Darja Kanduc, Jaume Alijotas-Reig, Vsevolod Zinserling, Natalia Semenova, Howard Amital, et al. Covid-19 and autoimmunity. *Autoimmunity reviews*, 19(8):102597, 2020.

Viktoria N Tsakalidou, Pavlina Mitsou, and George A Papakostas. Computer vision in autoimmune diseases diagnosis—current status and perspectives. In *Computational Vision and Bio-Inspired Computing*, pages 571–586. Springer, 2022.

I. S. Stafford, M Kellermann, E Mossotto, Robert Mark Beattie, Ben D. MacArthur, and Sarah Ennis. A systematic review of the applications of artificial intelligence and machine learning in autoimmune diseases. *NPJ Digital Medicine*, 3, 2020.

Anuroop Sriram, Matthew Muckley, Koustuv Sinha, Farah Shamout, Joelle Pineau, Krzysztof J. Geras, Lea Azour, Yindalon Aphinyanaphongs, Nafissa Yakubova, and William Moore. Covid-19 deterioration prediction via self-supervised representation learning and multi-image prediction, 2021.

Jun Cheng. brain tumor dataset. 4 2017. doi: 10.6084/m9.figshare.1512427.v5. URL https://figshare.com/articles/dataset/brain_tumor_dataset/1512427.

Jaeyong Kang, Zahid Ullah, and Jeonghwan Gwak. Mri-based brain tumor classification using ensemble of deep features and machine learning classifiers. *Sensors*, 21(6), 2021. ISSN 1424-8220. doi: 10.3390/s21062222. URL <https://www.mdpi.com/1424-8220/21/6/2222>.

Philipp Tschandl, Cliff Rosendahl, and Harald Kittler. The ham10000 dataset, a large collection of multi-source dermatoscopic images of common pigmented skin lesions. *Scientific Data*, 5, 2018.

David A. Gutman, Noel C. F. Codella, M. E. Celebi, Brian Helba, Michael Armando Marchetti, Nabin K. Mishra, and Allan C. Halpern. Skin lesion analysis toward melanoma detection: A challenge at the 2017 international symposium on biomedical imaging (isbi), hosted by the international skin imaging collaboration (isic). *2018 IEEE 15th International Symposium on Biomedical Imaging (ISBI 2018)*, pages 168–172, 2018.

Marc Combalia, Noel C. F. Codella, Veronica M Rotemberg, Brian Helba, Verónica Vilaplana, Ofer Reiter, Allan C. Halpern, Susana Puig, and Josep Malvehy. Bcn20000: Dermoscopic lesions in the wild. *ArXiv*, abs/1908.02288, 2019.

Mathilde Caron, Hugo Touvron, Ishan Misra, Hervé Jégou, Julien Mairal, Piotr Bojanowski, and Armand Joulin. Emerging properties in self-supervised vision transformers. In *Proceedings of the International Conference on Computer Vision (ICCV)*, 2021.

Jean-Bastien Grill, Florian Strub, Florent Altch'e, Corentin Tallec, Pierre H. Richemond, Elena Buchatskaya, Carl Doersch, Bernardo Ávila Pires, Zhaoan Daniel Guo, Mohammad Gheshlaghi Azar, Bilal Piot, Koray Kavukcuoglu, Rémi Munos, and Michal Valko. Bootstrap your own latent: A new approach to self-supervised learning. *ArXiv*, abs/2006.07733, 2020a.

Ting Chen, Simon Kornblith, Mohammad Norouzi, and Geoffrey Hinton. A simple framework for contrastive learning of visual representations. *arXiv preprint arXiv:2002.05709*, 2020a.

Shekoofeh Azizi, Basil Mustafa, Fiona Ryan, Zach Beaver, Jana von Freyberg, Jonathan Deaton, Aaron Loh, Alan Karthikesalingam, Simon Kornblith, Ting Chen, Vivek Natarajan, and Mohammad Norouzi. Big self-supervised models advance medical image classification. *2021 IEEE/CVF International Conference on Computer Vision (ICCV)*, pages 3458–3468, 2021a.

Asifullah Khan, Anabia Sohail, Umme Zahoor, and Aqsa Saeed Qureshi. A survey of the recent architectures of deep convolutional neural networks. *Artificial intelligence review*, 53(8):5455–5516, 2020.

Samir S Yadav and Shivajirao M Jadhav. Deep convolutional neural network based medical image classification for disease diagnosis. *Journal of Big Data*, 6(1):1–18, 2019.

Olaf Ronneberger, Philipp Fischer, and Thomas Brox. U-net: Convolutional networks for biomedical image segmentation. In *International Conference on Medical image computing and computer-assisted intervention*, pages 234–241. Springer, 2015.

Alexey Dosovitskiy, Lucas Beyer, Alexander Kolesnikov, Dirk Weissenborn, Xiaohua Zhai, Thomas Unterthiner, Mostafa Dehghani, Matthias Minderer, Georg Heigold, Sylvain Gelly, Jakob Uszkoreit, and Neil Houlsby. An image is worth 16x16 words: Transformers for image recognition at scale. *ArXiv*, abs/2010.11929, 2021.

Ze Liu, Yutong Lin, Yue Cao, Han Hu, Yixuan Wei, Zheng Zhang, Stephen Lin, and Baining Guo. Swin transformer: Hierarchical vision transformer using shifted windows. In *Proceedings of the IEEE/CVF International Conference on Computer Vision (ICCV)*, 2021a.

Ze Liu, Han Hu, Yutong Lin, Zhuliang Yao, Zhenda Xie, Yixuan Wei, Jia Ning, Yue Cao, Zheng Zhang, Li Dong, Furu Wei, and Baining Guo. Swin transformer v2: Scaling up capacity and resolution. In *International Conference on Computer Vision and Pattern Recognition (CVPR)*, 2022a.

Hugo Touvron, Matthieu Cord, Matthijs Douze, Francisco Massa, Alexandre Sablayrolles, and Hervé Jegou. Training data-efficient image transformers & distillation through attention. In *International Conference on Machine Learning*, volume 139, pages 10347–10357, July 2021.

Stéphane d’Ascoli, Hugo Touvron, Matthew Leavitt, Ari Morcos, Giulio Biroli, and Levent Sagun. Convit: Improving vision transformers with soft convolutional inductive biases. *arXiv preprint arXiv:2103.10697*, 2021.

Zhuang Liu, Hanzi Mao, Chao-Yuan Wu, Christoph Feichtenhofer, Trevor Darrell, and Saining Xie. A convnet for the 2020s. *Proceedings of the IEEE/CVF Conference on Computer Vision and Pattern Recognition (CVPR)*, 2022b.

Jean-Bastien Grill, Florian Strub, Florent Altché, Corentin Tallec, Pierre Richemond, Elena Buchatskaya, Carl Doersch, Bernardo Avila Pires, Zhaohan Guo, Mohammad Gheshlaghi Azar, Bilal Piot, koray kavukcuoglu, Remi Munos, and Michal Valko. Bootstrap your own latent - a new approach to self-supervised learning. In H. Larochelle, M. Ranzato, R. Hadsell, M.F. Balcan, and H. Lin, editors, *Advances in Neural Information Processing Systems*, volume 33, pages 21271–21284. Curran Associates, Inc., 2020b. URL <https://proceedings.neurips.cc/paper/2020/file/f3ada80d5c4ee70142b17b8192b2958e-Paper.pdf>.

Dan Hendrycks, Mantas Mazeika, Saurav Kadavath, and Dawn Song. Using self-supervised learning can improve model robustness and uncertainty. *Advances in Neural Information Processing Systems*, 32, 2019.

Mathilde Caron, Ishan Misra, Julien Mairal, Priya Goyal, Piotr Bojanowski, and Armand Joulin. Unsupervised learning of visual features by contrasting cluster assignments. *ArXiv*, abs/2006.09882, 2020.

Florin C Ghesu, Bogdan Georgescu, Awais Mansoor, Youngjin Yoo, Dominik Neumann, Pragneshkumar Patel, RS Vishwanath, James M Balter, Yue Cao, Sasa Grbic, et al. Self-supervised learning from 100 million medical images. *arXiv preprint arXiv:2201.01283*, 2022.

Shekoofeh Azizi, Basil Mustafa, Fiona Ryan, Zachary Beaver, Jan Freyberg, Jonathan Deaton, Aaron Loh, Alan Karthikesalingam, Simon Kornblith, Ting Chen, et al. Big self-supervised models advance medical image classification. In *Proceedings of the IEEE/CVF International Conference on Computer Vision*, pages 3478–3488, 2021b.

Christos Matsoukas, Johan Fredin Haslum, Magnus P Soderberg, and Kevin Smith. Is it time to replace cnns with transformers for medical images? *ArXiv*, abs/2108.09038, 2021.

Yu Liu, Amr H. Sawalha, and Qianjin Lu. Covid-19 and autoimmune diseases. *Current Opinion in Rheumatology*, 33:155 – 162, 2020.

Kaiming He, Haoqi Fan, Yuxin Wu, Saining Xie, and Ross B. Girshick. Momentum contrast for unsupervised visual representation learning. *2020 IEEE/CVF Conference on Computer Vision and Pattern Recognition (CVPR)*, pages 9726–9735, 2020.

Ting Chen, Simon Kornblith, Mohammad Norouzi, and Geoffrey E. Hinton. A simple framework for contrastive learning of visual representations. *ArXiv*, abs/2002.05709, 2020b.

Xinlei Chen and Kaiming He. Exploring simple siamese representation learning. *2021 IEEE/CVF Conference on Computer Vision and Pattern Recognition (CVPR)*, pages 15745–15753, 2021.

Maithra Raghu, Thomas Unterthiner, Simon Kornblith, Chiyuan Zhang, and Alexey Dosovitskiy. Do vision transformers see like convolutional neural networks? In *NeurIPS*, 2021.

Kaiming He, X. Zhang, Shaoqing Ren, and Jian Sun. Deep residual learning for image recognition. *2016 IEEE Conference on Computer Vision and Pattern Recognition (CVPR)*, pages 770–778, 2016.

Yuan Gong, Sameer Khurana, Andrew Rouditchenko, and James R. Glass. Cmkd: Cnn/transformer-based cross-model knowledge distillation for audio classification. *ArXiv*, abs/2203.06760, 2022.

Pavel Izmailov, Dmitrii Podoprikhin, T. Garipov, Dmitry P. Vetrov, and Andrew Gordon Wilson. Averaging weights leads to wider optima and better generalization. *ArXiv*, abs/1803.05407, 2018.

Tsung-Yi Lin, Priya Goyal, Ross B. Girshick, Kaiming He, and Piotr Dollár. Focal loss for dense object detection. *2017 IEEE International Conference on Computer Vision (ICCV)*, pages 2999–3007, 2017.

Kayla Van Buren, Yi Li, Fanghao Zhong, Yuan Ding, Amrutesh Puranik, Cynthia A. Loomis, Narges Razavian, and Timothy B. Niewold. Artificial intelligence and deep learning to map immune cell types in inflamed human tissue. *Journal of Immunological Methods*, 505:113233, 2022. ISSN 0022-1759. doi: <https://doi.org/10.1016/j.jim.2022.113233>. URL <https://www.sciencedirect.com/science/article/pii/S0022175922000205>.

Javeria Amin, Muhammad Almas Anjum, Muhammad Sharif, Saima Jabeen, Seifedine Kadry, and Pablo Moreno Ger. A new model for brain tumor detection using ensemble transfer learning and quantum variational classifier. *Computational Intelligence and Neuroscience*, 2022, 2022.

Ross Wightman. Pytorch image models. <https://github.com/rwightman/pytorch-image-models>, 2019.

Maithra Raghu, Chiyuan Zhang, Jon Kleinberg, and Samy Bengio. Transfusion: Understanding transfer learning for medical imaging. *Advances in neural information processing systems*, 32, 2019.

Ze Liu, Yutong Lin, Yue Cao, Han Hu, Yixuan Wei, Zheng Zhang, Stephen Lin, and Baining Guo. Swin transformer: Hierarchical vision transformer using shifted windows. In *Proceedings of the IEEE/CVF International Conference on Computer Vision (ICCV)*, pages 10012–10022, October 2021b.

Bill Cassidy, Connah Kendrick, Andrzej Brodzicki, Joanna Jaworek-Korjakowska, and Moi Hoon Yap. Analysis of the isic image datasets: usage, benchmarks and recommendations. *Medical Image Analysis*, 75:102305, 2022.

Nils Gessert, Maximilian Nielsen, Mohsin Shaikh, René Werner, and A. Schlaefer. Skin lesion classification using ensembles of multi-resolution efficientnets with meta data. *MethodsX*, 7, 2020.

David Picard. Torch. manual_seed (3407) is all you need: On the influence of random seeds in deep learning architectures for computer vision. *arXiv preprint arXiv:2109.08203*, 2021.

Jia Deng, Wei Dong, Richard Socher, Li-Jia Li, Kai Li, and Li Fei-Fei. Imagenet: A large-scale hierarchical image database. In *2009 IEEE conference on computer vision and pattern recognition*, pages 248–255. Ieee, 2009.